UvA-DARE (Digital Academic Repository)

The influence of mitoses rate on growth dynamics of a cellular automata model of tumour growth

Naumov, L.; Hoekstra, A.; Sloot, P.

Link to publication

International Conference on Computational Science, ICCS 2010

The influence of mitoses rate on growth dynamics of a cellular automata model of tumour growth

Lev Naumov*, Alfons Hoekstra, Peter Sloot

University of Amsterdam, Computational Science Science Park 107, 1098 XG, Amsterdam, The Netherlands

Abstract

Mitosis inside a tumour can be prohibited for different reasons, such as overcrowding or physical pressure. At the same time, the rate of successful mitoses inside a tumour can hardly be measured in vivo or vitro, but is easily modeled in silico. In this paper we present a study of the influence of mitoses rate on the growth dynamics of a cellular automata model for growth.
© 2010 Published by Elsevier Ltd.
Keywords: tumour, mitosis, cellular automata

1. Introduction

According to medical reports, cancer is the second leading cause of death in developed countries [1]. An effective scheme of its treatment is a research objective for many scientists, but not only biologists and clinicians participate in this process. Contemporary biological approaches and facilities are often not able to separate the underlying mechanisms of tumour growth, and here statistics and mathematical modeling make their contribution [2].

A rich variety of tumour growth models appeared in the last two decades [3–12]. Many of them use cellular automata [13–17] as a basic simulations vehicle, because these systems have proven their suitability and advantageous usability in the field of biomodeling [3].

In [18] we demonstrate the importance of taking natural tumour shrinkage due to necrosis of cells in the tumour mass into account in the simulation and its influence on the growth regime. Earlier cellular automata based mesoscopic models (which model a single biological cell by a single automaton cell) have not payed special attention to such shrinkage. Some involve it implicitly (in [19], for example), but a distinct rate of shrinkage was not determined.

The fact is that mitosis inside the tumour can be prohibited due to overcrowding, physical pressure, incoming intercellular signals or other reasons. A cell, which is situated deep inside the tumour, has less chance to divide successfully than one on the periphery of the tumour [20]. The rate of successful mitoses can hardly be observed and measured in vivo or in vitro. At the same time it can be easily simulated in silico. Our objective is to study the dependency of growth dynamics on this parameter.

We assume that the mitosis rate is uniformly distributed over the inner cells of the proliferating tumour layer. In vivo or in vitro this is different and there is a dependency between a chance to divide and the depth of the cell

---

*Corresponding author.
Email addresses: L.Naumov@uva.nl (Lev Naumov), A.G.Hoekstra@uva.nl (Alfons Hoekstra), P.M.A.Sloot@uva.nl (Peter Sloot)

disposition. While the exact character of this dependency is questionable, we decide to assume that the successful mitosis rate is the same for all cells inside the tumour. This assumption is not critical, accounting that a proliferating rim is usually several cells thick [21, 22].

In [18] the rate of successful mitoses is just given a certain value. Here, using the same experimental setup we will vary the rate and validate the results against in vitro growth of the LoVo cells spheroid [23], trying to make conclusions concerning the realism of distinct successful mitosis rates.

For the general avascular tumour simulation we will use one of the four variants of models, presented in [18], where natural tumour shrinkage was neglected and where chain shifting along straight lines was used for the expansion simulation [5, 7–10, 20, 24–26]. When a cell divides, it pushes one of its neighbours to free a place for its daughter cell. So, cells are pushed outwards one by one along a certain trajectory, starting from one of the mother cell's neighbours. In most cases this trajectory represents a straight line [7–10] or a random zigzag [27].

The scientific community has produced significant results and software [28, 29] for cellular automata based simulations. Our model was created with the help of the CAME$_\&$L software environment [29, 30].

2. Tumour Growth Model

The model is implemented with a three dimensional cellular automaton with Cartesian metrics and Moore's neighbourhood [31]. The timestep is equal to one hour. Each automaton's cell represents a single biological cell, with size $10\mu m \times 10\mu m \times 10\mu m$. Mersenne twister [32] was used for random numbers generation.

We assume that the metabolism requires one nutrient, which is diffusing from the healthy area into the clot of malignant cells. As a result, normal cells act as nutrition sources for the cancerous tissue. Diffusion is computed using a standard finite difference discretization of the diffusion equation.

We also assume homogeneous pressure, and neglect obstacles such as, for example, bones. So, the tumour expansion process in the model is organized as virtual "turning" of a normal cells into a malignant state.

The state data of the cellular automaton cell is divided into two parts: the first one describes a contained biological cell, whereas the second one characterizes an occupied area of tissue. The key difference between these two subsets is that elements of the first should "follow" the cell, when moves due to chain shifting. At the same time, the elements of the second one should not. The list bellow enumerates the fields from the first part.

1. *State* – Biological state of a cell. State N corresponds to a normal tissue cell. Values T_M, T_{G1}, T_S, T_{G2} designate different phases of a proliferating malignant cell's cycle, T_{G0} denote a quiescent malignant cell. A cell in state D represents the remains of a dead cell.

2. *InState* – The amount of timesteps, which a cell has spent in its current biological state. This value matters for proliferating and quiescent malignant cells only.

3. *PhaseDuration* – The amount of timesteps, which a current cell's phase has to last. This value also matters for proliferating and quiescent malignant cells only. This value should be calculated at the moment of the cell's transition to a new phase, according to known statistical data [33].

For the current version of the model, the set of fields, which describes the area of tissue occupied by a cell, consists of a single element: *NutrientConcentration* – local concentration of the nutrient.

The tumour growth simulation process is usually based on the assumption that the process starts from a single malignant cell [21], situated in the center of a grid. So, initially all cells of the grid contain normal biological cells, except the center one, which holds a malignant cell ready for mitosis (in T_M state).

A special list *ChainShiftOut* is used to store the coordinates of all the cells, which underwent mitosis on the current timestep. For each timestep the accumulating starts from scratch.

The rules, which govern the cellular automaton, can be separated into three logical elements: a prestep, an application of the transitions function (the step) and a poststep. The prestep contains the following operations:

- Increase the value of the *InState* field for all proliferating and quiescent malignant cells.

- Decrease the amount of available nutrients in the correspondence with the consumption rates for all proliferating and quiescent malignant cells.

- Clear *ChainShiftOut* list.

Below is a list of the transition conditions. They are arranged in order of execution. Note that if a cell's state was changed then the value of its *InState* field should be reset to zero.

1. $T_M \rightarrow T_{G1}$ (Mitosis) – If a cell is ready for mitosis, then its position inside the tumour should be checked. If there is a normal cell in its neighbourhood then the cell is considered to belong to tumour surface and its mitosis cannot fail. For inner cells mitosis can be successful with a given probability, which we will refer to as the successful mitoses rate. In case of the successful division the only thing to be done is to put the mother cell's coordinates in the *ChainShiftOut* list. The mother cell itself, being in the mitotic state, just continues to proliferate and enters the gap-1 phase [34].

2. $T_{G1} \rightarrow T_{G1}$; $T_S \rightarrow T_S$; $T_{G2} \rightarrow T_{G2}$ (Proliferation) – A cell stays in the current phase if its *InState* value is less than its *PhaseDuration* value [7–10, 34].

3. $T_{G1} \rightarrow T_S$; $T_S \rightarrow T_{G2}$; $T_{G2} \rightarrow T_M$ (Proliferation) – A cell changes the phase if its *InState* value reaches its *PhaseDuration* value [7–10, 34].

4. $T_{G1} \rightarrow T_{G0}$ (Getting quiescent) – A cell gets quiescent if the local level of the nutrient is below the per hour proliferating cell nutrient consumption rate [12].

5. $T_{G0} \rightarrow T_S$ (Returning from quiescence) – A cell returns from the quiescence to the proliferation if the local level of the nutrient is above the per hour proliferating cell nutrient consumption rate [12].

6. $T_{G0} \rightarrow D$ (Necrosis) – A cell dies if the supply of the nutrient have not appeared during the maximal quiescence time length [34].

7. $N \rightarrow N$ (Rest) – Normal cell is not changing its state by itself.

8. $T_{G0} \rightarrow T_{G0}$ (Quiescence) – Quiescent cell is not changing its state unless it returns to proliferation or dies [7–10, 12, 34].

9. $D \rightarrow D$ (Rest) – Dead cell is not changing its state by itself. This only can be caused by chain shifts.

The poststep consists in following operations:

- Diffuse the nutrient. Diffusion is much faster than the time step used to model the cell cycle. Therefore, at each time step we compute a steady state field of concentration of the nutrient.

- For each element of the *ChainShiftOut* list (which represents coordinates of a divided cell) perform the chain shift in random direction along a straight line and place a newborn cell in the T_{G1} phase to the disengaged cell (the first cell of the chain), which will be a mother cell's neighbour. Such kind of chain shift will definitely result in a fussy boundary of the formed clot. That is why it was decided to make one more operation: move the outermost malignant cell of the trajectory (the last cell of the chain) to one of its vacant neighbours, if the neighbour is closer to the geometrical center of the tumour. This imitates the pressure between the healthy tissue and the cancerous formation.

We will perform a number of experiments, varying the successful mitoses rate. Other parameters used for the simulations, the results and their agreement with the reality are presented in Sect. 3.

3. Experiments

3.1. Gompertz Law Based Validation

The kinetic behaviour of a tumour growth process can be reproduced by the Gompertz law [23, 35–38] which is widely used for these purposes. The law can be written in the following form:

$$V(t) = V_0 \exp\left(\frac{a}{b}\left(1 - \exp(-b\,t)\right)\right), \tag{1}$$

where $V(t)$ is the tumour volume in time; V_0 – the initial volume; a – the initial instantaneous tumour growth rate; b – the growth retardation factor.

Knowing V_0 it is possible to describe the growth regime with two values: *a* and *b*. The validation procedure consists in the comparison of these two parameters for the in silico data with the same values known for real in vitro or in vivo specimen.

At the same time, value of *a*/*b* ratio is also informative, regardless the exact values of *a* and *b*. It describes the growth pattern of the tumour: a larger ratio means that the growth is closer to the exponential one, while a smaller ratio points to more linear character of growth.

Demicheli et al. [23] report the following values for the in vitro growth of the mice LoVo cells spheroids:

$$a = 0.04 \pm 0.01 \quad \text{h}^{-1},$$
$$b = 0.0022 \pm 0.0007 \quad \text{h}^{-1}. \tag{2}$$

Moreover, they postulate a strong linear correlation between both parameters:

$$a = (7 \pm 1)\, b + (0.023 \pm 0.002). \tag{3}$$

Name	Comment (Measure)	Used Value
G1DurationMean	Malignant cell's gap-1 phase mean duration (in hours). In [33] durations of all phases of the murine sarcoma 180 cell's cycle are reported. The cycle duration for that type of tumour cells is 19.8 hours, while for mice LoVo cells it equals to 29.3 hours [39]. Values for the cell cycle phases for LoVo cells were obtained by proportional scaling from the values for murine sarcoma 180 cells.	12.3 h
SDurationMean	Malignant cell's DNA synthesis phase mean duration (in hours). For details see the *G1DurationMean* description.	12.5 h
G2DurationMean	Malignant cell's gap-2 phase mean duration (in hours). For details see the *G1DurationMean* description.	3.5 h
G0MaxDurationMean	Malignant cell's gap-0 phase mean duration (in hours). This value represents not the exact prolongation of the cell's quiescence, but the maximal possible duration of the dormancy. Value obtained from data published in [40]. Such order of magnitude is also presented in [41].	147.5 h
G1DurationSD	The standard deviation for the malignant cell's gap-1 phase duration (in hours). For details see the *G1DurationMean* description.	12.3 h
SDurationSD	The standard deviation for the malignant cell's DNA synthesis phase duration (in hours). For details see the *G1DurationMean* description.	3.75 h
G2DurationSD	The standard deviation for the malignant cell's gap-2 phase duration (in hours). For details see the *G1DurationMean* description.	1.4 h
G0MaxDurationSD	The standard deviation for the malignant cell's maximum gap-0 phase duration (in hours) [40].	30 h
NutrientConsumptionProlif	The amount of nutrient consumed by a proliferating malignant cell per hour (in grams per hour) [11].	$7.2 \cdot 10^{-11}$ g/h
NutrientConsumptionQuiesc	The amount of nutrient consumed by a quiescent malignant cell per hour (in grams per hour) [11].	$9.38 \cdot 10^{-12}$ g/h
NutrientDiffusion	Nutrient diffusion coefficient (in square meters per hour) [21].	$1.52 \cdot 10^{-7}$ m^2/h

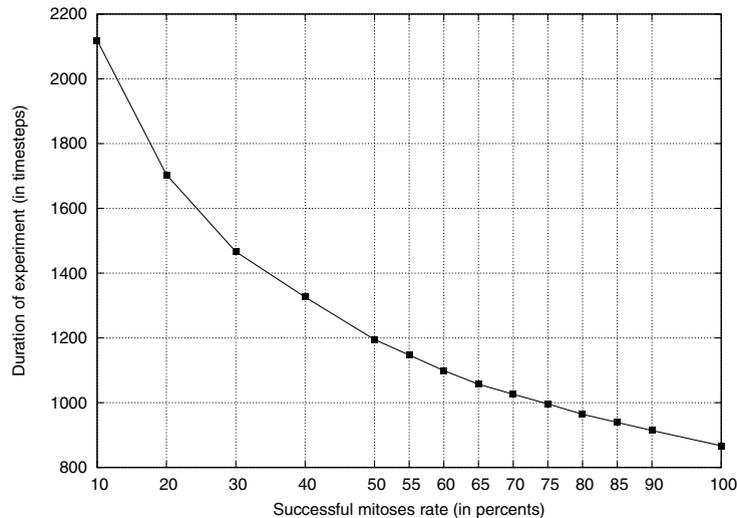Table 1: Model parameters and their values used for the experiments.

Figure 1: Amount of timesteps, needed for the modeled tumour to reach $201 \times 201 \times 201$ cells size versus the successful mitoses rates.

3.2. Experimental Setup

The set of model parameters reproduces the one used in [18] and corresponds to an in vitro tumour composed of LoVo cells. In Table 1 the parameters are presented with their values, which were used for the experiments.

These parameters were obtained from literature, which discuss in vivo or in vitro tumour growth experiments. We have studied the sensitivity of the model versus most of them varying their values by 1%. Model demonstrated its robustness.

3.3. Validation and Discussion

We have performed five experiments for each of following successful mitoses rates: 10%, 20%, 30%, 40%, 50%, 55%, 60%, 65%, 70%, 75%, 80%, 85%, 90%, and 100% (despite the last value not being realistic). The step is shortened between 50% and 90%, because, as we will demonstrate, this region represents the major interest. A grid of $201 \times 201 \times 201$ cells was used.

We measured the time (in cellular automaton steps) needed for the tumour to reach a $201 \times 201 \times 201$ cells size as a function of the successful mitoses rates. The results, averaged over the five experiments, are shown in Fig. 1.

For each experiment we fit the resulting growth curve versus the Gompertz law and retrieve a and b parameters. The maximal, minimal, and average values of a and b for a given successful mitoses rate are presented in Fig. 2. Starting with a successful mitoses rate of 20%, both Gompertzian growth parameters fall into the range of values as observed in vitro (see Eq. 2). At the same time, only starting from 60% almost all pairs of these parameters satisfy the linear correlation, given by Eq. 3. Only 2 of 40 experiments produce a and b values, which do not comply with it. At the same time, for a successful mitoses rate of 55% and below no single set of parameters pairs is in agreement with the linear correlation.

Having no ability to measure such microscopic parameter as the successful mitoses rate in real biological system, we can draw some conclusions about its magnitude, based on the simulation presented here and in vitro experiments of larger scale [23]. Our results suggest that at least 55% of inner proliferating tumour LoVo cells are dividing (see Fig. 3).

The global trends for a and b as function of the successful mitoses rate are as follows: a is growing, b is descending regardless the fluctuations. At the same time, both parameters are tightly interdependent. This is illustrated by the
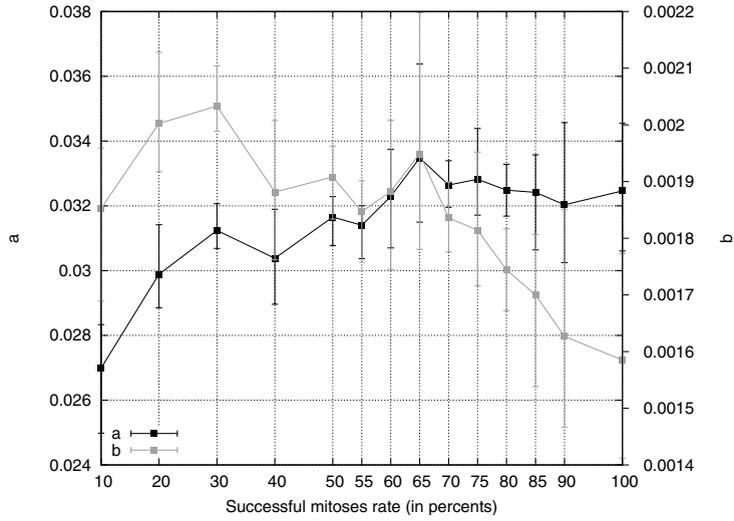
Figure 2: Maximal, minimal, and average values of *a* (shown in black) and *b* (shown in gray) versus the successful mitoses rates.
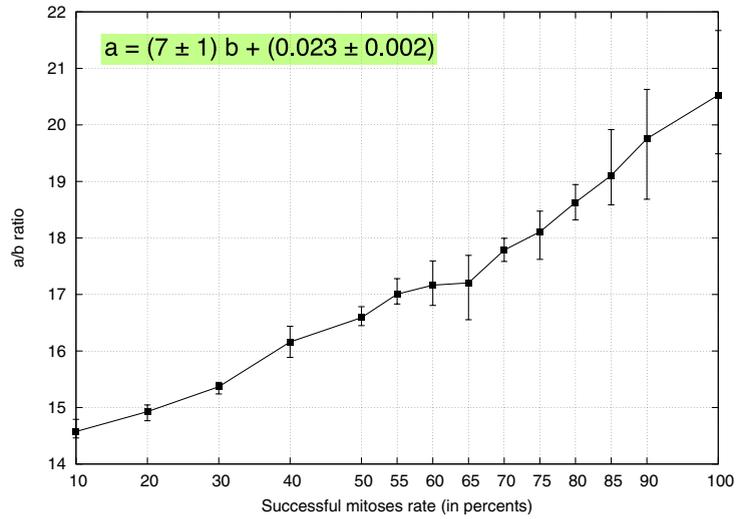

Figure 3: Maximal, minimal, and average values of *a/b* ratio versus the successful mitoses rates.

fact that their spreads (relative magnitude of difference between minimal and maximal values) and relative positions of the average values look similar for any given successful mitoses rate. Their interdependency results in the fact that the average a/b ratio is monotonously growing as one may see in Fig. 3. This conforms with the expectations that the growth should obtain more exponential character if the proportion of mitotic cells inside a tumour is increasing.

In [18] we use a value of the successful mitoses rate, which was computed during the simulations as a rate of the successful random walks from an inner malignant cell outside. A length of the walking trajectory was limited by a squared distance from the cell to the geometrical center of the tumour. Note, that the artificially computed result was 70% and this value belongs to the range of possible rates, according to the described research.

References

[1] World Health Organization, Fact sheet #297, Tech. rep., World Health Organization, http://www.who.int/mediacentre/factsheets/fs297/en/ (2008).
[2] L. A. Kunz-Schughart, M. Kreutz, R. Knuechel, Multicellular spheroids: A three-dimensional in vitro culture system to study tumour biology, International Journal of Experimental Pathology 79 (1998) 1–23.
[3] A. Deutsch, S. Dormann, Cellular Automaton Modeling of Biological Pattern Formation, Birkhäuser Boston, 2004.
[4] A. S. Qi, X. Zheng, C.-Y. Du, B.-S. An, A cellular automation model of cancerous growth, Journal of Theoretical Biology 161 (1993) 1–12.
[5] A. R. Kansal, S. Torquato, G. R. Harsh, E. A. Chiocca, T. S. Deisboeck, Simulated brain tumour growth dynamics using a three-dimensional cellular automation, Journal of Theoretical Bioliology 203 (2000) 367–382.
[6] M. Kocher, H. Treuer, J. Voges, M. Hoevels, V. Sturm, R. Mueller, Computer simulation of cytotoxic and vascular effects of radiosurgery in solid and necrotic brain metastases, Radiotherapy and Oncology 54 (2000) 149–156.
[7] G. S. Stamatakos, D. D. Dionysiou, E. I. Zacharaki, N. A. Mouravlinsky, K. S. Nikita, N. K. Uzunoglu, In silico radiation oncology: Combining novel simulation algorithms with current visualization techniques, Proceedings of IEEE 60 (2002) 1764–1777.
[8] D. D. Dionysiou, G. S. Stamatakos, N. K. Uzunoglu, K. S. Nikita, A. Marioli, A four-dimensional simulation model of tumour response to radiotherapy in vivo: Parametric validation considering radiosensitivity, genetic profile and fractionation, Journal of Theoretical Biology 230 (2004) 1–20.
[9] D. D. Dionysiou, G. S. Stamatakos, N. K. Uzunoglu, K. S. Nikita, A computer simulation of in vivo tumour growth and response to radio-therapy: New algorithms and parametric results, Computers in Biology and Medicine 36 (2006) 448–464.
[10] D. D. Dionysiou, G. S. Stamatakos, Applying a 4D multiscale in vivo tumour growth model to the exploration of radiotherapy scheduling: The effects of weekend treatment gaps and p53 gene status on the response of fast growing solid tumours, Cancer Informatics 2 (2006) 113–121.
[11] S. Dormann, A. Deutsch, Modeling of self-organized avascular tumour growth with a hybrid cellular automaton, In Silico Biology 2 (2002) 393–406.
[12] T. Alarcon, H. M. Byrne, P. K. Maini, A multiple scale model for tumour growth, Multiscale Modeling & Simulating 3 (2005) 440–475.
[13] J. von Neumann, The Theory of Self-reproducing Automata, University of Illinois Press, 1966.
[14] K. Zuse, Calculating Space, Massachusetts Institute of Technology Technical Translation AZT-70-164-GEMIT, Massachusetts Institute of Technology (Project MAC), 1970.
[15] S. Wolfram, A New Kind of Science, Wolfram Media Inc., 2002.
[16] P. Sarkar, A brief history of cellular automata, ACM Computing Surveys 32 (1) (2000) 1–23.
[17] P. M. A. Sloot, A. G. Hoekstra, Modeling dynamic systems with cellular automata, in: P. Fishwick (Ed.), Handbook of Dynamic System Modeling, Chapman & Hall/CRC, 2007, pp. 1–20.
[18] L. Naumov, A. Hoekstra, P. Sloot, Cellular automata models of tumour natural shrinkage, in preparation.
[19] A. A. Patel, E. T. Gawlinskia, S. K. Lemieuxe, R. A. Gatenby, A cellular automaton model of early tumor growth and invasion: The effects of native tissue vascularity and increased anaerobic tumor metabolism, Journal of Theoretical Biology 213 (2001) 315–331.
[20] D. Drasdo, Coarse graining in simulated cell populations, Advances in Complex Systems 8 (2005) 319–363.
[21] Y. Jiang, J. Pjesivac-Grbovic, C. Cantrell, J. P. Freyer, A multiscale model for avascular tumour growth, Biophysical Journal 89 (205) (2005) 3884–3894.
[22] E. I. Zacharaki, G. S. Stamatakos, K. S. Nikita, N. K. Uzunoglu, Simulating growth dynamics and radiation response of avascular tumour spheroids - model validation in the case of an emt6/ro multicellular spheroid, Computer Methods and Programs in Biomedicine 76 (3) (2004) 193–206.
[23] R. Demicheli, R. Foroni, A. Ingrosso, G. Pratesi, C. Soranzo, M. Tortoreto, An exponential-gompertzian description of lovo cell tumor growth from in vivo and in vitro data, Cancer Research 49 (1989) 6543–6546.
[24] M. L. Martins, S. C. F. Jr., M. J. Vilela, Multiscale models for the growth of avascular tumors, Physics of Life Reviews 4 (2007) 128–156.
[25] C. Harting, P. Peschke, K. Borkenstein, C. P. Karger, Single-cell-based computer simulation of the oxygen-dependent tumour response to irradiation, Physics in Medicine and Biology 52 (2007) 4775–4789.
[26] J. Smolle, Cellular automaton simulation of tumour growth equivocal relationships between simulation parameters and morphologic pattern features, Analytical Cellular Pathology 17 (1998) 71–82.
[27] A. Sottoriva, J. Verhoeff, T. Borovski, S. McWeeney, L. Naumov, J. Medema, P. Sloot, L. Vermeulen, Modeling cancer stem cell driven tumor growth reveals invasive morphology and increased phenotypical heterogeneity, Cancer ResearchIn press.
[28] T. Worsch, Programming environments for cellular automata, in: S. Bandini, G. Mauri (Eds.), Cellular Automata for Research and Industry (ACRI-1996), Springer-Verlag, 1996, pp. 3–12.
[29] L. Naumov, Generalized coordinates introduction method and a tool for computational experiments software design automation, based on cellular automata, Ph.D. thesis, Saint-Petersburg State University of Information Technologies, Mechanics and Optics (2007).

[30] L. Naumov, CAME&L – Cellular Automata Modeling Environment & Library, in: Cellular Automata: 6th International Conference on Cellular Automata for Research and Industry (ACRI-2004), Springer-Verlag, 2004, pp. 735–744.
[31] L. Naumov, Generalized coordinates for cellular automata grids, in: Computational Science - ICCS 2003. Part 2, Springer-Verlag, 2003, pp. 869–878.
[32] M. Matsumoto, T. Nishimura, Mersenne twister: a 623-dimensionally equidistributed uniform pseudo-random number generator, ACM Transactions on Modeling and Computer Simulation 8 (1) (1998) 3–30.
[33] K. Tornita, J. E. Plager, In vivo cell cycle synchronization of the murine sarcoma 180 tumour following alternating periods of hydroxyurea blockade and release, Cancer Research 39 (1979) 4407–4411.
[34] G. M. Fuller, D. Shields, Molecular Basis of Medical Cell Biology, Appleton and Lang, Stamford & Connecticut, 2006.
[35] G. Gompertz, On the nature of the function expressive of the law of human mortality and on the new mode of determining the value of life contingencies, Philosophical Transactions of the Royal Society of London 115 (1825) 513–585.
[36] A. K. Laird, Dynamics of growth in tumors and in normal organisms, Human Tumor Cell Kinetics 30 (1969) 15–28.
[37] L. Ferrante, S. Bompadre, L. Possati, L. Leone, Parameter estimation in a gompertzian stochastic model for tumor growth, Biometrics 56 (2000) 1076–1081.
[38] R. Chignola, R. Foroni, Estimating the growth kinetics of experimental tumors from a few as two determinations of tumor size: Implications for clinical oncology, IEEE Transactions on Biomedical Engineering 52 (2005) 808–815.
[39] J. J. Stragand, J.-P. Bergerat, R. A. White, J. Hokanson, B. Drewinko, Biological and cell kinetic properties of a human colonic adenocarcinoma (lovo) grown in athymic mice, Cancer Research 40 (1980) 2846–2852.
[40] M. Wartenberg, H. Diedershagen, J. Hescheler, H. Sauer, Growth stimulation versus induction of cell quiescence by hydrogen peroxide in prostate tumor spheroids is encoded by the duration of the Ca^{2+} response, The Journal of Biological Chemistry 274 (39) (1999) 27759–27767.
[41] F. Zolzer, C. Streffer, Quiescence in S-phase and G_1 arrest induced by irradiation and/or hyperthermia in six human tumour cell lines of different p53 status, International Journal of Radiation Biology 76 (5) (2000) 717–725.